SAND2000-1563C

Proceedings of NHTC '00
34th National Heat Transfer Conference
Pittsburgh, Pennsylvania, August 20-22, 2000

NHTC2000-12141

Determination of Thermal Conductivity of 304 Stainless Steel Using Parameter Estimation Techniques[1]

Bennie F. Blackwell[2], Walter Gill[3], Kevin J. Dowding[4], and Thomas E. Voth[4]
Sandia National Laboratories
Engineering Sciences Center
MS 0828
Albuquerque, NM 87185

ABSTRACT

Sensitivity coefficients were analyzed in order to guide the design of an experiment to estimate the thermal conductivity of 304 stainless steel. The uncertainty on the temperature measurements was estimated by several means and its impact on the estimated conductivity is discussed. The estimated thermal conductivity of 304 stainless steel is consistent with results from other sources.

NOMENCLATURE

c	specific heat, J/Kg-K
k	thermal conductivity, W/m-K
N_p	no. of parameters
N_s	no. of sensors
N_t	no. of measurement times
S	sum of squares function, see Eq. (6)
T	temperature, °C
T_k	scaled sensitivity coefficient, °C, see Eq. (1)
T_{max}	maximum temperature, °C
T_{min}	minimum temperature, °C
t	time, s
$\boldsymbol{X}$	sensitivity matrix
$\vec{x}$	position vector
Y_{ij}	temperature measurement for sensor i at time j, °C

Greek

Δ	D-optimality condition, see Eq. (4)
Δ^+	dimensionless D-optimality condition, see Eq. (5)
ΔT	$= T_{max} - T_{min}$
Δt	data sample rate
α	thermal diffusivity, m^2/s
ρ	density, Kg/m^3
$\hat{\sigma}_p$	estimated standard deviation in parameter p, units of p

INTRODUCTION

Thermal systems often incorporate a number of mechanical joints between individual components. These joints allow assembly/disassembly, furnish mechanical support, and provide pathways for redistribution of thermal energy. To predict the behavior of a thermal system, it is necessary to incorporate thermal contact phenomena into computational tools. An accepted modeling approach is to use correlations that provide contact conductance based on joint characteristics, such as material pair, surface finishes, surface hardnesses, and contact pressure. These parameters are important because the surface irregularities deform upon contact and control the actual interface area.

An experimental apparatus has been designed to develop contact conductance correlations for metal-to-metal interfaces. As part of the data reduction procedure, it is necessary to know the thermal conductivity of the metals on each side of the contact interface. This thermal conductivity information is often obtained from either handbooks or separate experiments designed to measure those values. An unpublished uncertainty analysis for the steady-state contact conductance experiment

1. Sandia is a multiprogram laboratory operated by Sandia Corporation, a Lockheed Martin Company, for the United States Department of Energy under Contract DE-AC04-94AL85000.
2. Distinguished Member of Technical Staff, Fellow ASME.
3. Principal Member of Technical Staff, Member ASME.
4. Senior Member of Technical Staff, Member ASME.

has indicated that the largest contributor is because of the uncertainty in the thermal conductivity of the metal. Also, a relative uncertainty of 10% on a handbook conductivity translates to a larger relative uncertainty in the estimated contact conductance. Therefore, it is important to reduce the uncertainty in the conductivity in order to reduce the uncertainty in contact conductance. In this paper we take an alternative approach in that we use the same basic hardware used in the contact conductance experiment to also measure the thermal conductivity. Since the thermal conductivity is measured on hardware that is prototypical for the contact conductance experiment, it is felt that the experimental uncertainty in the thermal conductivity measurements will be reduced over that obtained from a separate thermal conductivity experiment.

Description of Contact Conductance Experiment

A cutaway view of the contact conductance experiment is shown in Fig. 1. The contact interface of interest is that between the two hollow cylinders, each with an outside diameter of 8.89 cm (3.5 in), wall thickness of 0.508 cm (0.2 in), and length of 6.985 cm (2.75 in). (For the results reported here, a single continuous cylinder of 13.97 cm (5.5 in) length was used instead of the split cylinders. This cylinder was machined from the same billet as the split cylinders.) A flange of 12.7 cm (5.0 in) diameter by 0.635 cm (0.25 in) thickness is present on the upper and lower cylinder ends. The copper block is composed of two halves: the (solid) contact plate is 12.7 cm (5.0 in) diameter by 1.905 cm (0.75 in) thick; the body is 12.7 cm (5.0 in) diameter by 3.848 cm (1.515 in) and has serpentine channels machined in it to enhance the heat exchange effectiveness for the fluid circulated through it. The contact plate and body are brazed together and are referred to collectively as the copper block.

Time-dependent temperature measurements are provided by thermocouples mounted in the top and bottom copper blocks identified in Fig. 1. A single 30-gauge thermocouple (0.254 mm, 0.010 in diameter, Type K) measures the temperature of each of the copper blocks; this thermocouple is located 4.483 cm (1.765 in) from the copper/stainless steel flange interface (in the body) and at the bottom of a 6.35 cm (2.25 in) deep radial hole. Two separate temperature-controlled baths supply fluid to the top/bottom (OFHC) copper blocks. A simplified cross section of the heating/cooling blocks and stainless steel cylinder is shown in Fig. 2; for the experimental results presented here, a

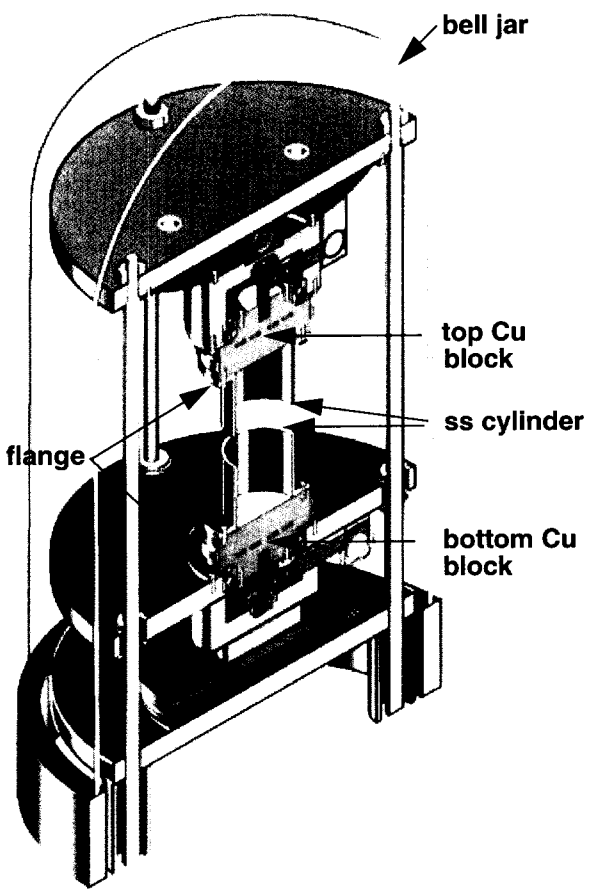

Figure 1. Cutaway view of contact conductance experiment

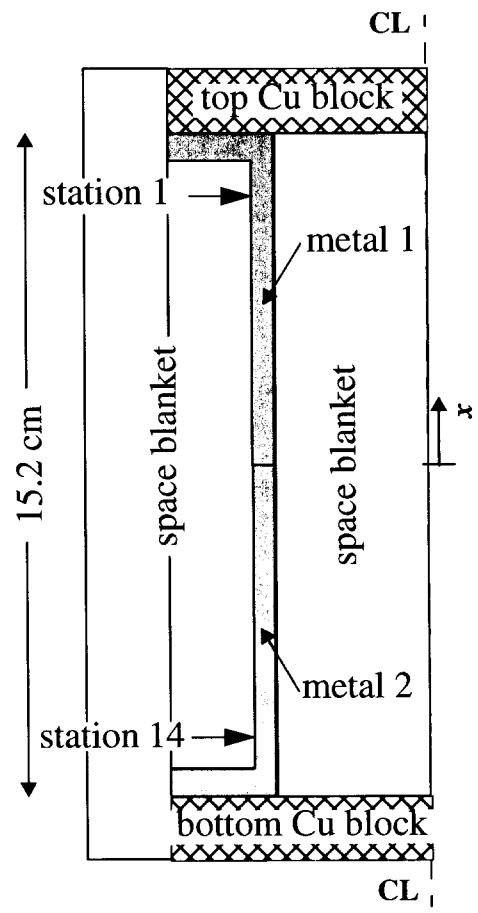

Figure 2. Cross section of experimental apparatus

continuous cylinder was used as opposed to the two piece cylinder shown in Fig. 2.

Thermocouples are mounted in the stainless steel cylinder walls at 14 axial stations with a uniform spacing of 0.953 cm (0.375 in). Station 1 is near the top of the cylinder and is located 0.795 cm (0.313 in) from the inside face of the flange. Station 14 is located at a mirror image position near the bottom flange. Stations 7 and 8 are located at ±0.475 cm (±0.187 in) from the $x = 0$ position (axial center line), respectively. At each axial station along the stainless steel cylinder, there are thermocouples at four angular stations, each 90 degrees apart for a total of 56 thermocouples mounted in the cylinder wall. The thermocouples are arranged in four columns: two columns of Type K and two columns of Type T, both of 30-gage wire (0.254 mm or 0.010 in diameter).

The thermocouples were installed by drilling 1.17 mm (0.0461 in) diameter by 2.54 mm (0.1 in) deep holes in the cylinder walls. The thermocouples were formed by stripping insulation from single-strand wire, welding the junction, and dipping the junction in a eutectic mix of indium/tin. The eutectic was also placed in the holes, and it remains liquid and ensures good contact between the thermoelectric elements and the stainless steel. The leads were wrapped around the outside diameter of the cylinder for one turn and held down with Kapton™ tape so as to minimize conduction losses along the lead wires.

The vacuum system consists of a bell jar vacuum chamber, a base plate with feed-through ports, and a complete vacuum pumping system with controls and gaging. The nominal dimensions of the glass bell jar vacuum chamber are 45.7 cm by 76.2 cm by 0.826 cm (18 in by 30 in by 0.325 in) wall thickness. The system is composed of a high-speed roughing pump and a four-stage diffusion pump capable of maintaining 10^{-7} Torr.

The data was acquired using the PC-based LabView™ with a 16 bit A-D system; the sample interval was one second.

EXPERIMENT DESIGN ISSUES

The temperature of the top and bottom copper blocks can be independently controlled through their own individual fluid baths; this allows considerable flexibility in the temperature history that can be imposed. Blackwell and Dowding (1999) explored optimum experiment design issues for the estimation of thermal conductivity from temperature data of this type. They considered two different boundary condition scenarios, termed "symmetric and "anti-symmetric" because of the boundary conditions imposed on the copper blocks. The "symmetric" boundary condition increased the temperature of both the top and bottom copper block by an amount ΔT, as rapidly as the temperature baths would allow. The "anti-symmetric" boundary condition increased the top Cu block temperature by $\Delta T/2$, whereas the lower block temperature was decreased by $\Delta T/2$. The temperature profile for the "symmetric" scenario is symmetrical about the midplane. Even if a midplane contacting surface was present, it would not impact the thermal conductivity estimation because of the presence of this symmetry or adiabatic surface. Furthermore, it was found that the symmetric scenario will have a smaller variance in the estimated conductivity than the anti-symmetric scenario. As such all results presented here will be for the "symmetric" boundary conditions.

The thermocouple results for a run at a pressure of roughly 4×10^{-5} Torr are shown in Fig. 3. This pressure is sufficiently low

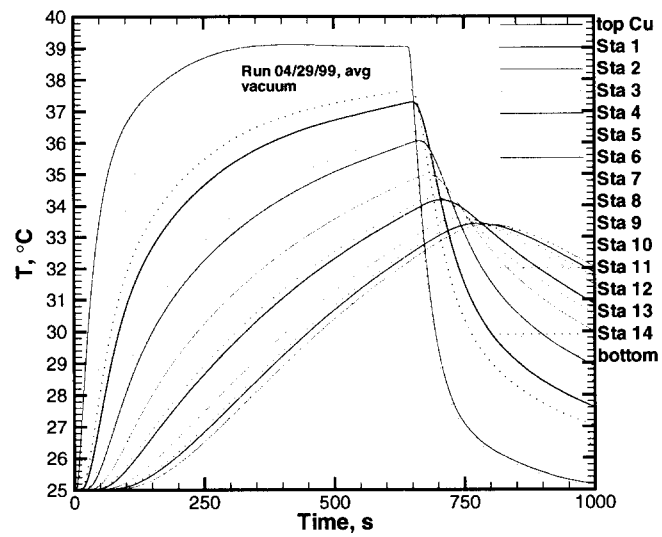

Figure 3. Experimental temperature results for Run 042999.

to eliminate convection, and the temperatures are sufficiently low that radiation is not significant. While the top and bottom copper block temperatures are from single thermocouple measurements, the Station 1-14 results are each the average of four thermocouples at the same axial station and equally spaced around the circumference of the cylinder. Statistics on these temperature measurements will be discussed in a subsequent section. Because of the finite capacity of the temperature baths, the change in temperature of the top and bottom copper blocks only approximates a step change boundary condition. Also, note that even though the top and bottom blocks were fed from the same temperature bath, their temperatures were not the same during the rapid transient. At early times the top block temperature may be as much as 4°C above the bottom block temperature. It is speculated that the reason for this discrepancy is that the piping lengths supplying the top and bottom Cu blocks are different. Had the top and bottom block temperature histories been the same, then pairs of thermocouples (Station 1 and Station 14, etc.) should also read the same. The farther the thermocouples are from the heated ends, the more closely the thermocouple pairs agree.

During the cool down phase, the thermocouple pairs on the

stainless steel cylinder cross over. The data reduction procedure to be discussed below will account for the fact that the top and bottom boundary conditions were different; longitudinal symmetry was not assumed.

The optimal design of experiments studies sensitivity coefficients in order to make decisions on quantities such as experiment duration, sensor locations, sample rate, etc. In this instance sensitivity coefficients are defined as partial derivatives of field variables (temperature in this case) with respect to parameters of interest (conductivity in this case). We have found it useful to utilize scaled sensitivity coefficients. For our experiments the scaled thermal conductivity sensitivity coefficient of interest is defined as

$$T_k(\vec{x}, t, k) = k\frac{\partial T}{\partial k}. \tag{1}$$

Note that the scaled sensitivity coefficient is a field variable just like temperature, and it has the units of temperature. The scaling of the sensitivity coefficient is important in that it allows sensitivity coefficients to be directly compared to a characteristic temperature rise of the experiment. For this experiment the characteristic temperature rise is the rise from its initial value. We utilized software designed specifically to compute both temperature and sensitivity coefficient fields. Details of this methodology can be found in Blackwell et al. (1999) and Dowding et al. (1999). This software utilizes a Control Volume Finite Element Method to solve the energy equation and also the derived sensitivity partial differential equations. It is felt that the sensitivity equation method is more accurate than finite difference determination of sensitivity coefficients and requires less user intervention to determine appropriate finite difference step sizes.

The computation of the temperature and sensitivity coefficient fields requires a computational mesh be developed for the experiment. If the copper blocks are included in the computational model, then the contact conductance between the top/bottom copper blocks and the stainless steel flanges must be included in this model. Two-dimensional simulations of the experiment were performed in which a range of copper/stainless steel contact conductances was assumed. From these calculations it was determined that the temperature field through the wall thickness at Stations 1 and 14 was uniform. This allows the geometrical extent of the model to be reduced to include only that portion of the cylinder between Stations 1 and 14 and eliminates the need for contact conductance at the copper/stainless steel interface. In fact, this says that the model is really one-dimensional as the boundary conditions are uniform at the Stations 1 and 14 cross sections. However, the data from this experiment was reduced using a two-dimensional axisymmetric computational model, since the software for computing the sensitivity coefficients did not have a 1-D model.

Sensitivity coefficients have been calculated for the 14 thermocouple stations. The results for Stations 1-7 are presented in Fig. 4 along with the temperature history at Station 1. Note

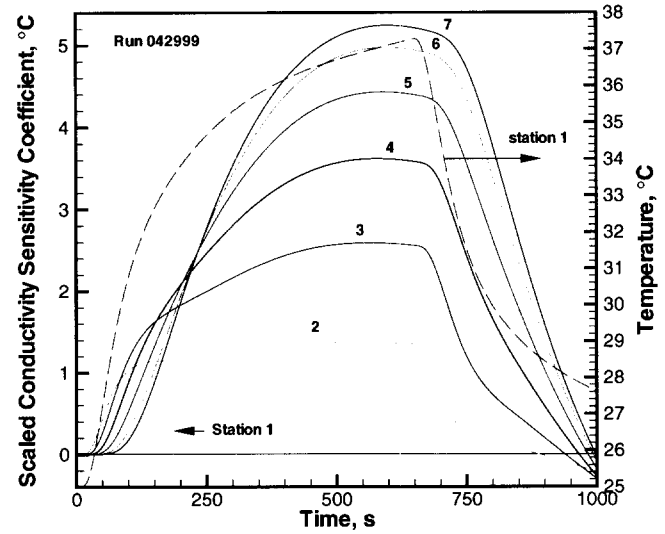

Figure 4. Scaled thermal conductivity sensitivity coefficients (left scale) and Station 1 temperature history (right scale).

that the sensitivity coefficient at Station 1 is zero; this is because the temperature at a specified temperature boundary condition is independent of the thermal conductivity. Station 7 has the largest sensitivity coefficient, indicating that it contributes the most information about the thermal conductivity. Since the thermocouple locations near the midplane of the experiment have the largest sensitivity coefficients, one might ask why the thermocouples were not located closer to the midplane. The original intent of the experiment was to measure the contact conductance using the steady state temperature profile and conductivity to estimate the heat flux. For this situation a uniform placement of thermocouples was thought to be better. The thermocouple locations were already specified before the conductivity estimation experiment was conceived. The sensitivity coefficient results for Stations 8-14 are very similar to those for Stations 1-7 and so are not shown.

The duration of the heating phase and cooling phase of Run 042999 (Fig. 3) was chosen based on engineering judgement and a visual inspection of the sensitivity coefficients. A more formal approach would involve optimal experiment design techniques. The D-optimality condition discussed in Beck and Arnold (1977) was used in subsequent analysis of the experiment design. This condition involves maximizing the determinant of the matrix

$$\Delta = \mathrm{Det}(\boldsymbol{X}^T\boldsymbol{X}), \tag{2}$$

where $\boldsymbol{X}$ is the $N_s \cdot N_t$ by N_p sensitivity matrix, the number of sensors is N_s, the number of times is N_t, and the number of

parameters is N_p. In this particular application, we are only estimating a single parameter, thermal conductivity of the stainless steel; hence $N_p = 1$. There are 14 sensors on the stainless steel cylinder, but since Stations 1 and 14 will be used as boundary conditions, there are only 12 axial stations contributing parameter estimation information; the sensitivity coefficients are zero at the specified temperature boundary conditions. The number of time measurements will be treated as variable through the relationship

$$t = N_t \Delta t, \tag{3}$$

where t is the experiment duration, and Δt is the data sample rate; for all the results presented here, $\Delta t = 1$ s. For this simple case of a single parameter, the optimality condition reduces to

$$\Delta = \sum_{i=1}^{N_s} \sum_{j=1}^{N_t} \left(\frac{\partial T}{\partial k}\bigg|_{i,j} \right)^2 . \tag{4}$$

One could increase Δ by adding sensors or taking more measurements as long as $\partial T/\partial k$ is nonzero. Furthermore, because $\partial T/\partial k$ is typically related to the temperature range, a larger temperature variation causes Δ to increase. To eliminate these dependencies, a normalized version of the optimality condition was used in this study and is defined to be

$$\Delta^+ = \frac{1}{N_s N_t (T_{max} - T_{min})^2} \sum_{i=1}^{N_s} \sum_{j=1}^{N_t} \left(k \frac{\partial T}{\partial k}\bigg|_{i,j} \right)^2 , \tag{5}$$

where (T_{max}, T_{min}) is the (maximum, minimum) temperature over time and sensor location. The quantity Δ^+ can be viewed as an information content per data sample, and we want to choose the heating and cooling durations that maximize this quantity. The time dependence of Δ^+ comes through the implicit dependence of N_t on time, Eq. (3).

Note the presence of the scaled thermal conductivity sensitivity coefficients in Eq. (5). These scaled sensitivity coefficients are precisely those shown in Fig. 4. When the cooling phase is initiated (by means of a temperature boundary condition), there is no sudden increase or decrease in sensitivity coefficients as there is when experiments are driven with a heat flux boundary condition, and the heat flux is turned off. Consequently, the cooling phase does not add much additional information in the situation being studied here.

The D-optimality condition defined in Eq. (5) for Run 042999 is presented in Fig. 5. The heating duration for this experiment was 644 s; beginning at this time cooling fluid was circulated through the top and bottom copper blocks. The cooling duration can be treated as a variable to be selected based on the time at which Δ^+ in Fig. 5 is a maximum; this time is 756 s. Even

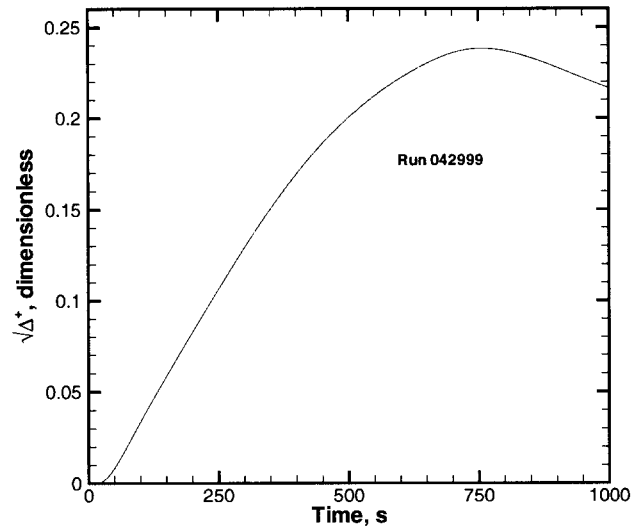

Figure 5. D-optimality condition as a function of time.

though the experiment was run in excess of 1000 s, the majority of the information about thermal conductivity is contained in the first 756 s of the experiment. The data was reduced using a run duration of 1000s.

THERMAL CONDUCTIVITY ESTIMATION

The thermal conductivity is estimated from the experimental temperatures in Fig. 3 such that the least square error between the computational model of the experiment and the experimental temperatures is minimized. This sum of squares function is given by

$$S = \sum_{i=1}^{N_s} \sum_{j=1}^{N_t} (T_{ij} - Y_{ij})^2 . \tag{6}$$

The iterative solution to this minimization problem was accomplished through the DAKOTA (1999) software, which allows one to connect stand-alone thermal analysis software with stand-alone optimization software. The communication between the various software is through external data files. This approach allows the thermal analysis software and optimization software to develop independent of each other. Additional details on this approach have been presented in Blackwell and Eldred (1997) and Dowding and Blackwell (1998).

The computational model consisted of the walls of the stainless steel cylinder. The end boundary conditions were the experimentally measured temperatures at Stations 1 and 14. The boundary conditions on the side walls of the cylinder were adiabatic. The estimated thermal conductivity was 14.34 W/m-K; this result compares favorably with other measurements

given in Table 1; the other measurements were linearly

Table 1: Comparison of thermal conductivity of 304 Stainless Steel with other results. Units are W/m-K and are valid for 31°C; uncertainty bound is ±2σ

This Work	Taylor, et al. (1997)	Incropera and De Witt (1990)
14.34±0.58	14.74±1.5	14.97

interpolated at a temperature of 31°C, the average temperature of Run 042999. The uncertainty statement contained in Taylor, et al. (1997) stated that the conductivity was accurate to ±5%. It is not known if this uncertainty bound was 1σ or 2σ; it was assumed to be 1σ. The details of the uncertainty analysis for this work are presented below.

Since time-dependent temperature data is used in the parameter estimation process, the computational model requires both thermal conductivity and volumetric heat capacity. The use of temperature boundary conditions to drive the model precluded the possibility of estimating both conductivity and volumetric heat capacity from the temperature measurements presented here. The conductivity estimation process was performed by assuming a value for the volumetric heat capacity and then minimizing the least square error. If the volumetric heat capacity is arbitrarily changed, then the resulting conductivity estimate will also change such that the ratio (thermal diffusivity) is a constant. Consequently, the parameter estimation process really estimates the thermal diffusivity. The density and heat capacity values used in the data reduction process were ρ = 7916±18 Kg/m^3 (this work, 1σ) and c= 497±10 J/Kg-K (Taylor et al., 1997; given as 2% accuracy, assumed to be 1σ).

Beck and Arnold (1977) indicate that for additive, uncorrelated errors with zero mean, the standard deviation in the estimated thermal diffusivity is related to the standard deviation in the temperature measurements through

$$\hat{\sigma}_\alpha^2 = \frac{1}{\Delta}\hat{\sigma}_T^2, \text{ or } \hat{\sigma}_\alpha = \frac{1}{\sqrt{\Delta}}\hat{\sigma}_T . \tag{7}$$

This relationship points out why maximizing Δ is important in terms of minimizing the errors in the estimated conductivity. The dimensional and dimensionless Δ are related through Eq. (4) and Eq. (5) and can be written as

$$\Delta = \frac{N_s N_t \Delta T^2}{\alpha^2}\Delta^+ . \tag{8}$$

The variance and standard deviation in the estimated conductivity can be written as

$$\left(\frac{\hat{\sigma}_\alpha}{\alpha}\right)^2 = \frac{1}{N_s N_t \Delta^+}\left(\frac{\hat{\sigma}_T}{\Delta T}\right)^2, \text{ or } \frac{\hat{\sigma}_\alpha}{\alpha} = \frac{1}{\sqrt{N_s N_t \Delta^+}}\frac{\hat{\sigma}_T}{\Delta T}. \tag{9}$$

The issue we are faced with now is how to estimate $\hat{\sigma}_T$. This will be explored in more detail in the following section.

ESTIMATES OF STANDARD DEVIATION IN TEMPERATURE MEASUREMENTS

It is important to study the temperature residuals corresponding to the estimated thermal diffusivity. These residuals are an indicator of the standard deviation in temperature and are defined as the difference between the experiment and the model temperatures. Residuals for Run 042999 are presented in Fig. 6. The standard deviation in the

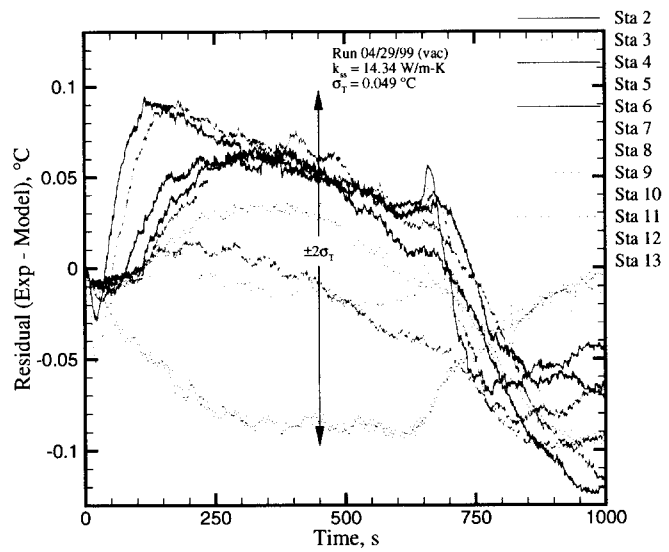

Figure 6. Temperature residuals for Run 042999.

temperature can be estimated from

$$\hat{\sigma}_T^2 = \frac{1}{N_s N_t - 1}\sum_{i=1}^{N_s}\sum_{j=1}^{N_t}(T_{ij} - Y_{ij})^2 \tag{10}$$

and was found to be 0.049°C. Visually the band of $\pm 2\hat{\sigma}_T$ in Fig. 6 appears to capture 95% of the residuals. Ideally the residuals should be randomly distributed around zero. Clearly the residuals in Fig. 6 are not random, suggesting that there may be inconsistencies between the measurements and the computational model. Most likely this pattern is because of the model not including all the physics present in the experiment. However, note the small magnitude of the residuals, indicating good agreement between the model and data.

At steady state, uncertainty in the temperature measurement is because of random noise from the data acquisition system and fixed bias from the data acquisition amplifiers or variations in thermocouple alloy composition. To assess the noise level and simultaneously remove the bias, the instrumented cylinder was subjected to long-term soaking at constant temperature levels in a temperature-controlled oven. A thermistor with a calibration

traceable to NIST was installed on the cylinder, and its temperature was used to develop a thermocouple-by-thermocouple correction curve for bias errors. Because the thermocouples were installed on the parts and connected to the data acquisition system as in the actual experiment, the correction represents an end-to-end calibration of the temperature measurement system. Bias corrections were on the order of 0.5°C and varied with thermocouple. The remaining error (assumed to be random noise) amounted to roughly $\hat{\sigma}_T = \pm 0.10$°C over all the thermocouples.

For dynamic temperature measurements, such as reported here, an additional source of uncertainty is the installation of the thermocouple in the cylinder wall. First, the thermocouple, being of finite size and installed in a metal part with a temperature gradient, leads to ambiguities in interpreting its reading. Further, nonperfect contact between the thermocouple and the well in which it was installed coupled with the difference in thermocouple wire material properties leads to a time lag in the reading. Thus the uncertainty in the dynamic situation is dependant on installation details, the local time rate of change of temperature, and the local thermal gradient in the cylinder. To quantify the contribution of these effects to uncertainty, the time response of the four circumferential thermocouples at each axial station were compared by calculating the standard deviation about the station mean at each data time. These results are shown in Figure 7 for axial Stations

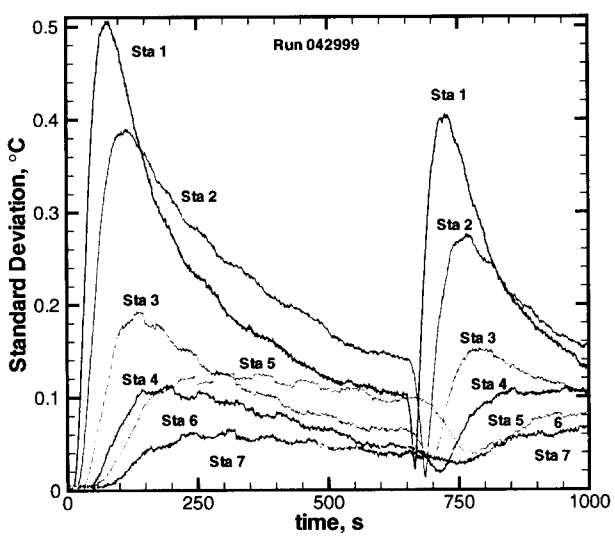

Figure 7. Standard deviation in four circumferential stations for axial stations 1-7

1-7; similar results were obtained for axial Stations 8-14. It was found that for axial stations closest to the boundary (1-3), which underwent relatively high rates of change in high-gradient conditions, the spatial standard deviation was as high as 0.5°C (Station 1) to about 0.2°C (Station 3). For the other stations the spatial standard deviation was at or below 0.10°C, when steady state was approached. Note that the sensors with the largest errors (Stations 1-3 and 12-14) have the smallest thermal conductivity sensitivity coefficient (see Fig. 4).

There is a strong correlation between temperature rise rate, temperature gradient, and circumferential standard deviation. The temperature rise rate and the temperature gradient for Station 1 were computed using the experimental data and finite differences, and these results are given in Fig. 8. The peak spatial temperature gradient lags the peak temperature rise rate. The peak in the standard deviation curve (taken from Fig. 7 for Station 1) occurs at a time between when the maximum time and spatial temperature gradients occur. The maximum temperature gradient at Station 1 is approximately 0.28°C/mm. For a thermocouple well of 1.17 mm diameter, the position of the 0.254 mm (0.010 in) diameter wire pair could vary by as much as ±0.44 mm (±0.017 in); this assumes that the two wires are side by side in a direction perpendicular to the axis of the cylinder. Using the above (maximum) temperature gradient of 0.28°C/mm and the positional uncertainty of the center line of the thermocouple wire, the uncertainty in temperature is approximately ±0.12°C; this result is consistent with the near steady-state results presented in Figure 7. This result does not consider that the presence of the thermocouple alters the temperature one is trying to measure.

In summary, the three temperature uncertainty estimates vary by an order of magnitude and lie in the approximate range

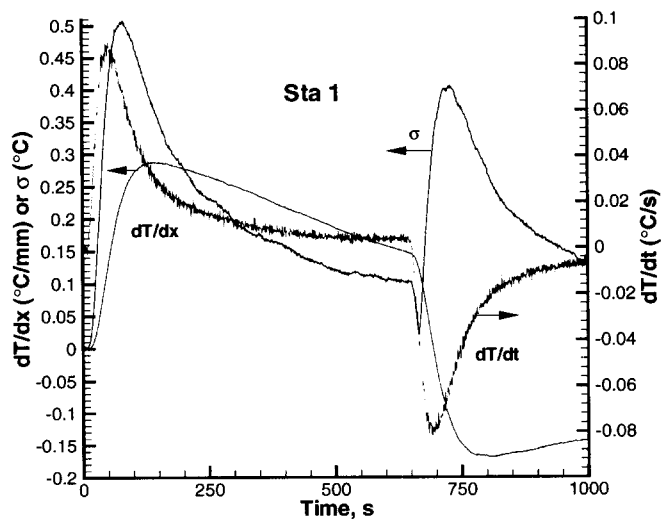

Figure 8. Temperature gradient, temperature rise rate, and circumferential standard deviation for axial Station 1.

$0.05 < \hat{\sigma}_T < 0.5$ °C. These results are summarized in Table 2.

Table 2: Estimated standard deviation in temperature using various methods

method	$\pm 1\hat{\sigma}_T$, °C
residual	0.049
steady state	0.10
maximum circumferential average	0.5

UNCERTAINTY IN ESTIMATED THERMAL CONDUCTIVITY

To account for the uncertainty in the estimated thermal conductivity, we focus on the relationship between the thermal conductivity, thermal diffusivity, density, and specific heat

$$k = \alpha\rho c. \tag{11}$$

The uncertainty in the conductivity is related to the uncertainty in the other parameters through

$$\left(\frac{\hat{\sigma}_k}{k}\right)^2 = \left(\frac{\hat{\sigma}_\alpha}{\alpha}\right)^2 + \left(\frac{\hat{\sigma}_\rho}{\rho}\right)^2 + \left(\frac{\hat{\sigma}_c}{c}\right)^2. \tag{12}$$

The estimated uncertainty in the thermal diffusivity can be obtained from Eq. (9), yielding

$$\left(\frac{\hat{\sigma}_k}{k}\right)^2 = \frac{1}{N_s N_t \Delta^+}\left(\frac{\hat{\sigma}_T}{\Delta T}\right)^2 + \left(\frac{\hat{\sigma}_\rho}{\rho}\right)^2 + \left(\frac{\hat{\sigma}_c}{c}\right)^2. \tag{13}$$

Utilizing the most pessimistic estimate for the standard deviation in temperature (0.5°C) and the other parameters for this experiment, Eq. (13) yields

$$\left(\frac{\hat{\sigma}_k}{k}\right)^2 = 5.8x10^{-7} + 5.2x10^{-6} + 4.0x10^{-4}. \tag{14}$$

Clearly the uncertainty in the specific heat dominates the uncertainty in the thermal conductivity. The final estimated thermal conductivity is

$$k = 14.34 \pm 0.58 \text{ W/m-K } (\pm 2\sigma \text{ bounds}). \tag{15}$$

Any further reductions in uncertainty in thermal conductivity estimate must be accompanied by a reduction in the (2%) uncertainty in the specific heat.

SUMMARY

An experiment to measure contact conductance between axially and tangentially loaded hollow cylinders has been described. In order to minimize the uncertainty in contact conductance because of uncertainty in thermal conductivity, a companion experiment was developed to measure thermal conductivity using prototypical hardware of the contact conductance experiment. The experimental configuration was axial heat conduction in the walls of a hollow cylinder. Optimum experiment design issues were discussed. Sensitivity coefficients and the D-optimality condition were computed. The estimated thermal conductivity at 31°C was 14.34 W/m-K, which compares favorably with other estimates. An uncertainty analysis on the temperature measurements was performed using three different methods with the results given in Table 2. The uncertainty in the specific heat is the dominant factor in the conductivity uncertainty. In order to further reduce the uncertainty in the contact conductance that is to be measured in future experiments, the uncertainty in the estimated heat capacity will have to be reduced.

ACKNOWLEDGMENTS

The authors acknowledge the support of Pat Drozda and Chuck Hanks of Sandia for the fabrication of the apparatus, writing of the data acquisition software, and conduct of the experiments.

REFERENCES

Beck, J. V. and Arnold, K. J., 1977, *Parameter Estimation in Engineering and Science*, Wiley, New York.

Blackwell, B. F. and Eldred, M. S., 1997, "Application of Reusable Interface Technology for Thermal Parameter Estimation, in G. S. Dulikravich and K. A. Woodbury (eds), *Proceedings 32nd National Heat Transfer Conference*, vol. 2, Inverse Problems in Heat Transfer and Fluid Flow,"ASME HTD-Vol. 340, pp. 1-8.

Blackwell, Bennie F. and Dowding, Kevin J, 1999, "Sensitivity Analysis and Uncertainty Propagation in a General Purpose Thermal Analysis Code," *Proceedings of the 3rd ASME/JSME Joint Fluids Engineering Conference*, July 18-23, San Francisco, CA.

Blackwell, Bennie F., Dowding, Kevin J., and Cochran, Robert J., 1999, "Development and Implementation of Sensitivity Coefficient Equations for Heat Conduction Problems," *Numerical Heat Transfer*, Part B, Vol 36, pp 15-32.

DAKOTA, 1999, DAKOTA Iterator Toolkit, World Wide Web URL: http://endo.sandia.gov/9234/sd_optim_dakota.html.

Dowding, K. J. and Blackwell, B. F., 1998, "Joint Experimental/ Computational Techniques to Measure Thermal Properties of Solids," *Measurement Science and Technology*, Vol. 9, No. 6, pp. 877-887.

Incropera, Frank P. and De Witt, David P., 1990, *Introduction to Heat Transfer*, 2nd Edition, Wiley, NY.

Taylor, R. E., Groot, H., and Ferrier, J., 1997, "Thermophysical Properties of SS 304," *TPRL 1904*, Thermophysical Properties Research Laboratory, Purdue University.